# Support Effect in Oxide Catalysis: Methanol Oxidation on Vanadia/Ceria

Thomas Kropp, Joachim Paier, and Joachim Sauer*

Institut für Chemie, Humboldt-Universität zu Berlin, Unter den Linden 6, 10099 Berlin, Germany

S *Supporting Information*

ABSTRACT: Density functional theory is used for periodic models of monomeric vanadia species deposited on the $CeO_2(111)$ surface to study dissociative adsorption of methanol and its subsequent dehydrogenation to formaldehyde. Dispersion-corrected PBE+U calculations are performed and compared with HSE and B3LYP results. Dissociative adsorption of methanol at different sites on $VO_2 \cdot CeO_2(111)$ is highly exothermic with adsorption energies of 1.8 to 1.9 eV (HSE+D). Two relevant pathways for desorption of formaldehyde are found with intrinsic

barriers for the redox step of 1.0 and 1.4 eV (HSE+D). The calculated desorption temperatures (370 and 495 K) explain the peaks observed in temperature-programmed desorption experiments. Different sites of the supported catalyst system are involved in the two pathways: (i) methanol can chemisorb on the CeO_2 surface filling a so-called pseudovacancy and the H atom is transferred to an V−O−Ce interphase bond or (ii) CH_3OH may chemisorb at the V−O−Ce interphase bond and form a V−OCH_3 species from which H is transferred to the ceria surface, providing evidence for true cooperativity. In both cases, ceria is directly involved in the redox process, as two electrons are accommodated in Ce f states forming two Ce^{3+} ions whereas vanadium remains fully oxidized (V^{5+}).
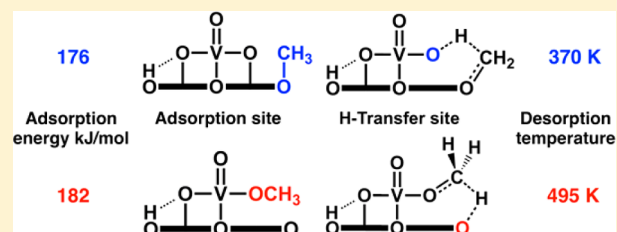
1. INTRODUCTION

Solid catalysts are complex systems with the active component dispersed on a supporting oxide. Heterogeneous catalysis provides ample evidence for the important role of the support for the activity and selectivity of a catalyst.[1,2] As a recent example, several orders of magnitude activity changes have been observed for CO oxidation on Pt nanoparticles supported on different oxides.[3] Here, we deal with transition metal oxides as industrially relevant catalysts that activate C−H bonds. Over more than a decade, evidence has been gathered[4−6] for a 3 to 4 orders of magnitude change in activity for, e.g., vanadium oxide supported on a broad variety of reducible and nonreducible oxides,[7] but an atomistic understanding has not yet been achieved. The reported results are for the partial oxidation of methanol to formaldehyde, but for the partial oxidation of ethanol and the oxidative dehydrogenation of propane the same observations have been made.[8,9] It has also been inferred that the support determines the type and distribution of the vanadia species and that these differences are the reason for the variation in turnover frequencies with the support for a given vanadium loading.[8,10]

Ceria-supported transition metal oxide catalysts are particularly active. Recent experimental and theoretical studies, including surface science experiments on model catalysts,[9,11−13] point to a very special role of this support.[14] It stabilizes the reduced state of the catalyst by accommodating electrons in the cerium f states, while vanadium remains in its highest oxidation state. This redox participation of the surroundings of an active M=O site in the C−H bond activation has also been found in

enzymes. In cytochrome P450 which selectively oxidizes C−H bonds to C−OH bonds, the porphyrin ligand of the active Fe^{IV}=O species also participates in the redox reaction.[15] This may be considered a *unifying concept* in catalysis.

The above-mentioned and other results raise doubts about attempts[7,16] to ascribe the observed activity changes to the V−O−M interphase bond only (M − metal of the supporting oxide) and to map the support effect to one parameter such as Sanderson's electronegativity. While the higher activity of ceria-supported catalysts compared to nonreducible supports such as alumina and silica has been rationalized[9,13] by means of the energy of oxygen defect formation as a descriptor,[17,18] detailed information on how the support interferes with the elementary reaction steps is still missing. This is the subject of the present computational study. Specifically, for the methanol oxidation we will examine which of the available sites participate in the initial chemisorption step and in the hydrogen transfer step: the V=O site, the V−O−M interphase sites, or sites at the supporting oxides. To reduce complexity connected with varying size distribution for different supports,[8,10] in this study we focus on monomeric vanadia species and, hence, do not consider V−O−V sites. A previous study on silica-supported vanadia showed that larger species are more reactive,[19] whereas for vanadia on ceria the opposite was predicted.[20]

For the vanadia/silica system[21] a previous computational study of monomeric sites (later confirmed and augmented)[22] has shown that first methanol chemisorbs on the V−O−Si interphase bond as also inferred from experiments.[23] Subsequently, a hydrogen atom is transferred from the methoxy group to the vanadyl (V=O) bond (see Figure 1). The latter is
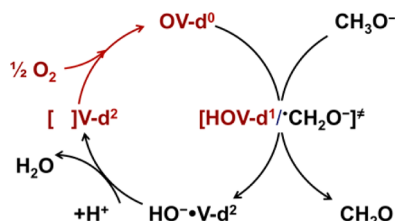

Figure 1. Mars−van Krevelen catalytic cycle for the methanol oxidation at a silica-supported vanadia species.

the rate-determining redox step involving a biradicaloid transition structure with vanadium in the +4 oxidation state (d^1 electron configuration on V). On release of CH_2O, another electron is transferred to vanadium, which acquires a d^2 electron configuration (+3 oxidation state). After water desorption, the reduced catalyst features an oxygen vacancy. The catalytic cycle is completed by a reoxidation step (Mars−van Krevelen),[24] the details of which have also been studied computationally.[25]

For monomeric vanadia species on ceria, we use a periodic model of VO_2 adsorbed on the $CeO_2(111)$ surface (see Figure 2). DFT+U calculations[26] showed that VO_2 is the most stable
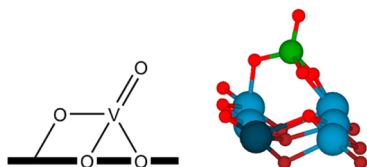

Figure 2. VO_2 deposited on the $CeO_2(111)$ surface. The ball and stick model (right) uses the following color code: Ce^{4+} (blue), Ce^{3+} (dark blue), O (red; subsurface dark red), and V (green).

VO_n species under the slightly reducing conditions of the model catalyst experiments.[11] Vanadia is stabilized in its +5 oxidation state, and electrons are transferred to CeO_2 as indicated by DFT+U and XPS.[11] Therefore, our surface model features a Ce^{3+} ion which is always present in addition to the one or two Ce^{3+} ions formed in the catalytic cycle. It also features a cavity in the $CeO_2(111)$ surface, which we refer to as a pseudovacancy[27] and which turns out to be a strong adsorption site. Driven by the strong preference of vanadium for a tetrahedral coordination, the deposited VO_2 species pulls an oxygen ion out of the surface which creates the cavity.

We have found six different chemisorption structures for methanol. For two of the most stable adsorption structures that can form without a barrier we have studied possible reaction pathways. For each of them, two transition structures have been identified as well as a number of intermediates on the way to the final products. Similarly to results for vanadia supported on (reducible) titania[28] (see also refs 29−31), the pathways with the lowest apparent energy barriers directly involve the support. In the first one, methanol chemisorbs at the V−O−Ce interphase bond and forms a V−OCH_3 species whose hydrogen atom is transferred to the ceria surface. In the alternative pathway methanol chemisorbs on the ceria surface

and the hydrogen atom is transferred to the V−O−Ce interphase bond. In both cases, the transition structure features a Ce^{3+} ion (in addition to the one already present in $VO_2/CeO_2(111)$), while vanadium stays +5. In the fully reduced state of the catalyst, there are two additional Ce^{3+} ions. Integration of the Polanyi−Wigner desorption equation for these two pathways using calculated desorption energies and pre-exponentials yields two peaks that explain the temperature-programmed desorption (TPD) features observed for the $VO_x/CeO_2(111)$ model catalyst.[13] We conclude that changing the support may change the active sites, and redox-active supports may be directly involved in the redox step.

Density functional theory (DFT) is applied with the Perdew−Burke−Ernzerhof functional[32] augmented by a dispersion term.[33,34] Attention is paid to the proper description of electrons in vanadium d and cerium f states ("DFT+U")[35,36] and to the possible existence of broken-symmetry open shell low-spin states as "biradicaloid" transition states. Comparison with hybrid functionals is also made.

2. COMPUTATIONAL DETAILS

Calculations were performed using the projector augmented wave (PAW) method[37,38] as implemented in the Vienna *ab initio* simulation package (VASP).[39,40] The onsite Coulomb correlation of occupied f orbitals is corrected with the DFT+U[35,36] approach employing the exchange-correlation functional of Perdew, Burke, and Ernzerhof (PBE)[41] and an effective Hubbard-type U parameter of 4.5 eV for the Ce $4f$ electrons, i.e. PBE+U. This U value was calculated self-consistently by Fabris et al.[42] A value between 3.0 and 5.5 eV leads to a proper localization of the two electrons left upon oxygen removal from CeO_2.[43] The specific implementation of DFT+U used in this work follows Dudarev et al.[44,45] Selected structures were also calculated using the hybrid functional by Heyd, Scuseria, and Ernzerhof (HSE)[46] as well as B3LYP.[47,48] A plane wave kinetic energy cutoff of 600 eV was used, and structure optimizations were performed until forces acting on the relaxed atoms were below 0.02 eV Å^{-1} for PBE+U and 0.04 eV Å^{-1} for hybrid functional calculations. The plane wave cutoff determining the Fourier grid for the Fock exchange related routines was set to $^9/_4$ times the cutoff for expanding the orbitals. The vanadium PBE pseudopotential includes the [Ar]-core $3p$ states in the valence space. The semiempirical C_6/R^6 term by Grimme (DFT+D2) was added to correct for missing long-range dispersion-type interactions.[33,34] The required van der Waals parameters for Ce were taken from ref 20. The global scaling parameter s_6 was 0.75, 0.6, and 1.05 for PBE+U, HSE, and B3LYP, respectively. Based on the PBE+U results, dispersion correction affects structural parameters only to a minor degree. Thus, when HSE and B3LYP results are reported, these are results of single-point calculations for the respective DFT+D structures.

The oxygen-terminated $p(4 \times 4)$ surface unit cell was generated cutting bulk CeO_2 in (111) orientation with cell vectors that amount to 15.518 Å (PBE+U), 15.266 Å (HSE), and 15.452 Å (B3LYP), respectively. Our slab model consists of nine atomic layers ($Ce_{48}O_{96}$), where the bottom trilayer is frozen to simulate the bulk. The vacuum layer was set to 10 Å. Because of the large cell, sampling of the Brillouin zone was restricted to the Γ point.

Optimized structures using PBE+U were proven to be minima by the absence of imaginary vibrational frequencies. Calculations of harmonic frequencies include all atoms, but the frozen bottom trilayer. The force constants are calculated as numerical derivative of forces with atomic displacements of ±0.015 Å. Zero-point vibrational energy (ZPVE) contributions are calculated from these frequencies.

Transition structures were obtained by nudged elastic band (NEB) calculations[49,50] in combination with the so-called climbing image method[51] as implemented in VASP. The improved dimer method (IDM) was used to refine these structures.[52,53]

The ball-and-stick models in Figures 2, 3, and 6 were generated using VESTA[54] with the following color code: C (black), Ce^{4+} (blue), Ce^{3+} (dark blue), H (white), O (red; subsurface dark red), and V (green).
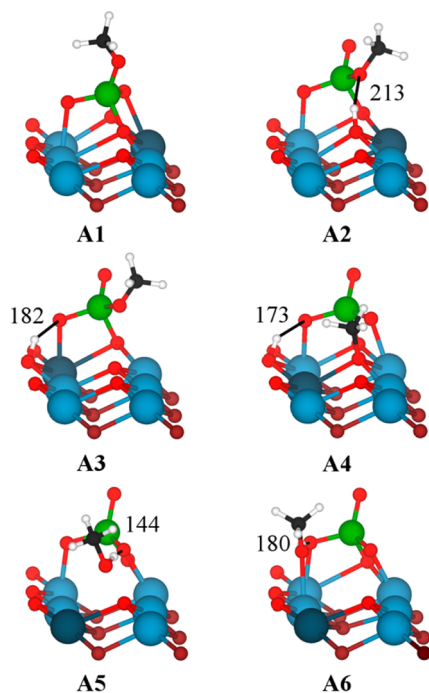

Figure 3. Adsorption structures **A1**−**A6** with hydrogen bond lengths in pm. Additional colors include C (black) and H (white).

3. RESULTS

3.1. Methanol Adsorption. Figure 2 shows the tetrahedral coordination of the monomeric vanadia surface species. It contains a vanadyl group ($r_{V=O}$ = 163 pm) and two different types of interphase oxygen atoms. One connects V to a surface cerium atom (r_{V-O} = 174 pm), and two are surface oxygen atoms (O_s) to which VO_2 is attached with its V atom (r_{V-O} = 181 pm). Methanol can adsorb by insertion into an interphase bond or into the pseudovacancy that opens in the surface when VO_2 is attached to the surface oxygen atoms. Figure 3 shows six different adsorption structures, and Table 1 lists their energies.

Table 1. Adsorption Energies Including Zero-Point Vibrational Energies, ΔE_0, for Methanol in eV

	PBE+U+D	D//PBE+U+D[a]
A1	−1.89	−0.20
A2	−1.72	−0.27
A3	−1.71	−0.29
A4	−1.77	−0.32
A5	−1.32	−0.30
A6	−0.95	−0.15

[a]Dispersion contribution at the PBE+U+D structure.

Structure **A1** is formed by chemisorption of CH_3OH onto a V−$O_{surface}$ bond. It is similar to the structure found by Sauer and co-workers[21] for silica-supported vanadia. Vanadium stays tetrahedrally coordinated, but the VO_4 tetrahedron moves 25 pm up. One of the surface O atoms is replaced by the oxygen atom in the methoxide, and the vanadyl oxygen atom attaches

to a Ce surface atom. Hence, this structure does not contain a vanadyl V=O bond anymore. The two V−O (Ce) interphase bonds are shorter (171/167 pm) than in the surface vanadia species. Upon methanol adsorption, the Ce^{3+} ion formed on VO_2 deposition[26] localizes next to the hydroxyl group located on the CeO_2 surface. The latter forms a hydrogen bond (172 pm) with the longer (171 pm) of the V−O interphase bond.

This structure is found to be the most stable one with an adsorption energy of −1.89 eV, but its formation requires significant structural rearrangements leading to a barrier of at least 0.6 eV as estimated by NEB runs.

Structure **A2** obtained by inserting methanol into a V−O interphase bond is slightly less stable (−1.71 eV). The methoxide replaces an anchoring oxygen atom, which relaxes into the pseudovacancy. The hydroxyl group, located next to the Ce^{3+} site, forms a weak hydrogen bond with the methoxide oxygen atom with a H⋯O distance of 213 pm (see Figure 3). Structure **A3** is structurally and energetically very close to **A2**, although the sites for the Ce^{3+} ion and the hydroxyl group are different. Conversion of both structures into each other appears to be easy with a low barrier of approximately 0.5 eV (see ref 55). It consists of a mere relocation of the hydroxyl H atom, which interacts with the interphase O atom (182 pm).

Structure **A4** is fundamentally different as methanol adsorbs into the pseudovacancy. Dispersion stabilizes this adsorption structure more than the other ones (Table 1), but the total adsorption energy (−1.77 eV) is comparable to the values for **A2** or **A3**. The methoxide oxygen atom is located 34 pm above the topmost surface layer, which is slightly higher than the hydroxyl oxygen atom (31 pm). Ce^{3+} is located between the hydroxyl group and the methoxide. Whereas the V=O group is still present, similar to **A1**, two nearly equivalent interphase oxygen atoms are formed, one of which interacts with the hydroxyl H atom (173 pm).

In structure **A5**, methanol is molecularly adsorbed. It forms a hydrogen bond (136 pm) to the elevated anchoring oxygen atom of the VO_2 unit, and its oxygen is 89 pm above the pseudovacancy, which is thus partially healed. Although structure **A5** is the most stable molecular adsorption structure found, dissociation into **A4** is favored by 0.4 eV. Since the corresponding barrier is only 0.08 eV, molecular adsorption structures should not be present on a (dehydrated) catalyst.

A second molecular adsorption structure **A6** was found to be significantly less stable. Methanol adsorbs atop of a Ce^{4+} ion with a hydrogen bond (171 pm) to an interphase oxygen atom, and stabilization by relaxation is minor.

3.2. Formaldehyde Formation. The most stable adsorption structures presented in the previous section are obvious starting points for various methanol oxidation pathways, and for each adsorption structure, multiple oxidation pathways are possible. Starting with **A1**, hydrogen transfer to one of the interphase oxygen atoms leads to intrinsic barriers greater than 2.0 eV and is, therefore, not relevant. Hydrogenation energies indicate that hydrogen transfer to surface oxygen atoms would be more favorable,[20] but these are too far away for this adsorption structure.

Starting with **A2** or **A3**, the hydrogen atom can either be transferred to the vanadyl group, the interphase oxygen atom, or a CeO_2 surface oxygen atom (**A3** only). In the present work, different hydrogen transfer pathways starting with **A3** (methoxide bonded to V) and **A4** (methoxide in pseudovacancy) are investigated using PBE+U and hybrid functionals. Reaction pathways starting with **A2** and **A3** feature similar
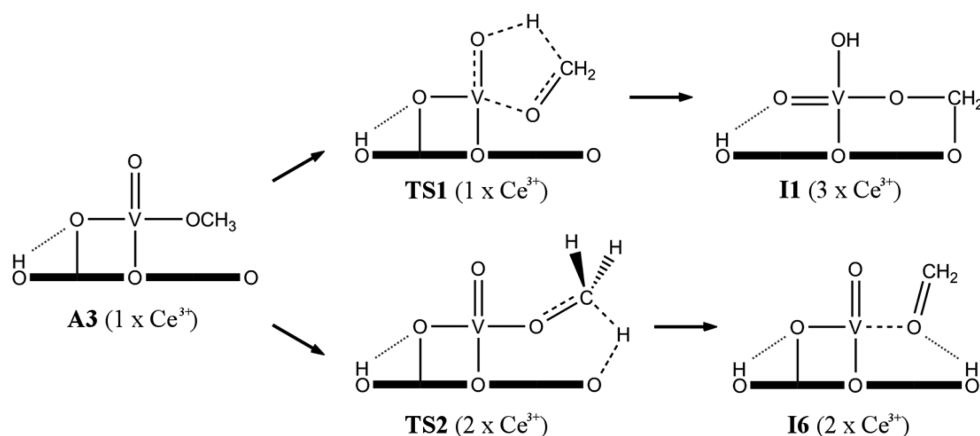
Figure 4. Hydrogen transfer step starting with **A3**. Top row: transfer to the vanadyl group; bottom row: transfer to a surface oxygen atom. Dotted lines represent hydrogen bonds, whereas dashed lines represent delocalized electrons.

transition structures, but the intrinsic barriers for **A2** are roughly 0.2 eV higher. Therefore, reaction channels involving **A2** will not be mentioned explicitly. Total energies discussed in this section are corrected for ZPVE and include dispersion (PBE+U+D). The ZPVE contributions decrease barriers by at most 0.2 eV, but do not affect reaction energies significantly.

3.2.1. Vanadium-Bonded Methoxide (A3). Figure 4 shows intermediates and transition structures for hydrogen transfer to the vanadyl group and to a CeO$_2$ surface oxygen atom starting with **A3**, and Table 2 reports selected bond distances. Figure 5

Table 2. Selected Bond Distances (pm) for the Structures Shown in Figure 4 Obtained with PBE+U+D

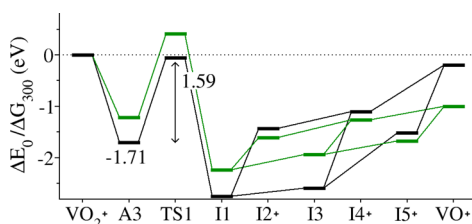| bond	A3	TS1	I1	TS2	I6	I3
OH···O	177	182	203	195	187	146
V−O	172	169	164	171	169	177
V=O	162	172	180	163	163	162
V−OC	183	188	181	185	196	186
O−C	143	141	147	137	129	141
C−H	110	153	−	139	−	−
O−H	−	128	97	121	97	97

Figure 5. PBE+U+D reaction energy profile (ZPVE-corrected) with vanadyl O as the H-accepting atom and **A3** as the starting structure. Gibbs free energies (green) have been calculated for 300 K and 0.1 MPa. The plus sign after some structures indicates that the reported energies include gas phase molecules, e.g. CH$_3$OH for **VO$_2$**+ or CH$_2$O for **I2**+.

shows the reaction energy profile for the hydrogen transfer to the vanadyl group. The transition structure **TS1** consists of a distorted five-membered ring. The imaginary mode (1502 cm^{-1}) shows that the hydrogen transfer is accompanied by planarization of the CH$_2$O moiety, which then bends toward the ceria surface. The barrier of this step (1.65 eV) results in a slightly negative apparent barrier of −0.06 eV.

Structure **A3** features one unpaired electron (doublet state), the Ce *f* electron stemming from the deposition of VO$_2$. In the transition structure, this is the highest occupied orbital defining the Fermi level. A spin-unpolarized calculation with a pseudopotential excluding the Ce *f* states from the valence bands affects the barrier by less than 0.04 eV and thus proves the role of this Ce^{3+} ion as an "innocent spectator" in this reaction. The second highest occupied orbital (2.0 eV below the Fermi level) is populated by two electrons of opposite spin. Its delocalization over the five-membered ring (see Figure 6)
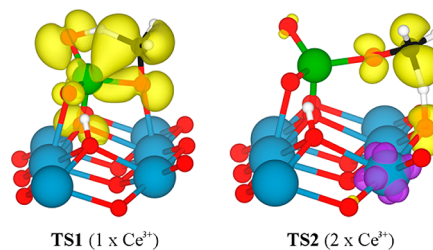

Figure 6. Electron density isocontour (0.01 Å^{-3}) for the second highest occupied orbital of **TS1** and spin density isocontour (0.01 Å^{-3}) for positive (yellow) and negative (purple) spin densities of **TS2**.

points to a concerted mechanism. The projected electron density shows that the vanadium d_{yz} state is partially populated and overlaps with the π* orbital of the CH$_2$O moiety. Since, for this transition structure, the ceria support is redox-innocent, it does not come as a surprise that the barrier coincides with the one reported by Sauer and co-workers[21] for the methanol oxidation on vanadia supported on the nonreducible silica.

Relaxation of **TS1** yields intermediate **I1**, which contains a V−O−CH$_2$−O−Ce moiety, i.e. formaldehyde coordinated to both VO$_X$ (r$_{V-O}$ = 181 pm) and the ceria support (r$_{C-O}$ = 138 pm). This structural motif is thermodynamically highly favored over V···O═CH$_2$ present in the vanadia/silica system. The oxidation step is strongly exothermic (−1.04 eV). Upon relaxation, both electrons occupying the delocalized orbital of the five-membered ring are transferred into Ce 4*f* states. Here, we see true cooperativity between vanadia and the support: the CH$_3$O$^-$ species formed in the chemisorption step has transferred a proton to the vanadyl group and two electrons to the ceria support.

The various pathways available for CH$_2$O desorption are also shown in Figure 5, and the corresponding structural schemes
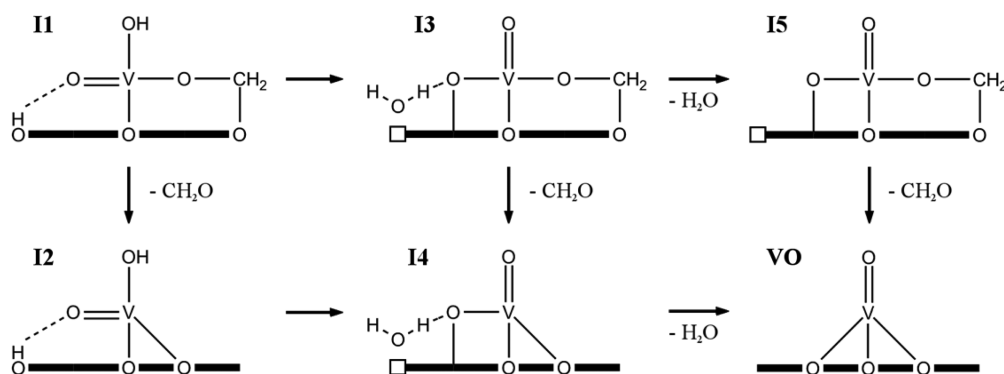
Figure 7. Elementary steps involved in water and formaldehyde desorption starting with **I1**. All these intermediates contain three Ce^{3+} ions; no electron transfer between vanadia and ceria occurs during the desorption steps.

are presented in Figure 7. Each route contains the following elementary steps: formaldehyde desorption (**I1** → **I2**, **I3** → **I4**, **I5** → **VO**), water formation (**I1** → **I3**, **I2** → **I4**), and water desorption (**I3** → **I5**, **I4** → **VO**). None of these pathways seems to be favored over another, especially when considering free energies, and may occur simultaneously. The desorbing formaldehyde will contain either the methanol oxygen atom or a surface oxygen atom. The former pathway would require the formation of an under-coordinated vanadium, which involves very high barriers;[27] the desorbing formaldehyde is more likely to contain a surface oxygen atom. Such an oxygen exchange in the primary product of the methanol oxidation was observed by Romanyshyn et al. at the $V_2O_5(001)$ surface via isotope labeling.[56]

Figure 8 shows the reaction energy profile for hydrogen transfer to a CeO_2 surface oxygen atom starting from the same
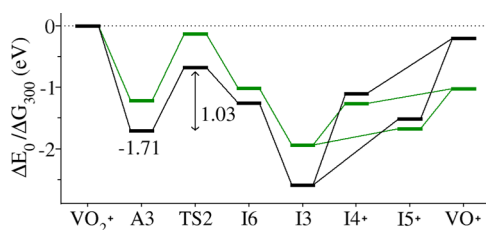

Figure 8. PBE+U+D reaction energy profile (ZPVE-corrected) with surface O as the H-accepting atom and **A3** as the starting structure. Gibbs free energies (green) have been calculated for 300 K and 0.1 MPa. For some structures, the plus sign indicates that the reported energies include gas phase molecules, e.g. CH_3OH for **VO₂+**.

adsorption structure (**A3**). Following the trend in hydrogenation energies, -1.34 eV for vanadyl groups and -1.51 eV for surface oxagen atoms,[20] the intrinsic barrier for **TS2** (1.03 eV) is much lower than that for **TS1**. The apparent barrier is as low as -0.68 eV. The imaginary mode belonging to the transition structure **TS2** (1464 cm^{-1}) also features the planarization of CH_2O in addition to the hydrogen transfer.

In the **TS2** transition structure (Figure 4), the electron has been transferred into a Ce f orbital and the proton to a surface oxygen atom. The electronic structure corresponds to an antiferromagnetically coupled low-spin state (broken-symmetry solution). One of these orbitals (purple isocontour in Figure 6) is mostly Ce f, resulting in a second Ce^{3+} ion in addition to the innocent one. The other state (yellow isocontour in Figure 6) corresponds to the π^* orbital of formaldehyde, but also extends into the ceria surface. This is similar to what has been found for

the H transfer to the vanadyl oxygen atom at silica-supported vanadia,[21] in which case the electron is transferred into a V d orbital, and the proton to the vanadyl oxygen atom. However, the intrinsic barrier is much lower. Obviously, accommodating electrons into Ce f states instead of vanadium d states is energetically more favorable, which is in agreement with previous findings.[13,26]

Relaxation of **TS2** leads to intermediate **I6**, which contains a partially reduced vanadium atom (V^{+4}) with some electron delocalization into the formaldehyde π^* orbital (backbonding). This intermediate contains the above-mentioned $V\cdots O=CH_2$ motif, while the stable $V-O-CH_2-O-Ce$ structure is only formed upon water formation (intermediate **I3**, Figure 8). During this process, an electron moves from V d to Ce f, resulting in two Ce^{3+} (plus one innocent one) compared to one Ce^{3+} (plus one innocent one) in **I6**.

3.2.2. Methoxide Bonded in the Pseudovacancy (A4). Starting with methoxide bonded in the pseudovacancy (**A4**), hydrogen can be transferred to one of the interphase oxygen atoms or a CeO_2 surface oxygen atom. The latter was not investigated since this pathway is expected to be very similar to the oxidation of methanol adsorbed in an oxygen vacancy of $CeO_2(111)$ as described in ref 57. Figure 9 shows two pathways for hydrogen transfer which differ in the accepting interphase oxygen atom, more distant from the methoxide (**TS3**) or closer to it (**TS4**). Selected bond distances are given in Table 3.

The hydrogenation energy is the same in both cases,[20] and the lower barrier is obtained for the closer distance between hydrogen and the accepting oxygen atom. Here, the simple electronic reactivity descriptor that does not consider the local structure of the active site faces its limits.

Transition structure **TS3** is reached from **A4** upon rotation of the $O=VO_3$ tetrahedron toward the adsorbed methoxide species. Along this rotation, the more distant interphase oxygen atom detaches from the ceria surface inducing electron transfer into the Ce $4f$ states. Thus, a second Ce^{3+} ion is created in the surface in addition to the one already present. The other unpaired electron (antiparallel spins) is delocalized over the interphase oxygen p state and the CH_2O π^* state. The imaginary mode (1501 cm^{-1}) involves planarization of CH_2O as well as the H transfer. In addition, the hydrogen bond to the surface hydroxyl group is weakened as indicated by bond elongation (see Table 3). The apparent barrier and the reaction energy for **A4** → **I3** are -0.68 and -1.01 eV, respectively. Figure 10 shows the entire energy profile.

Structure **I3** is reached from **TS3** by hydrogen transfer to the surface hydroxyl group forming water (Figure 9). No local
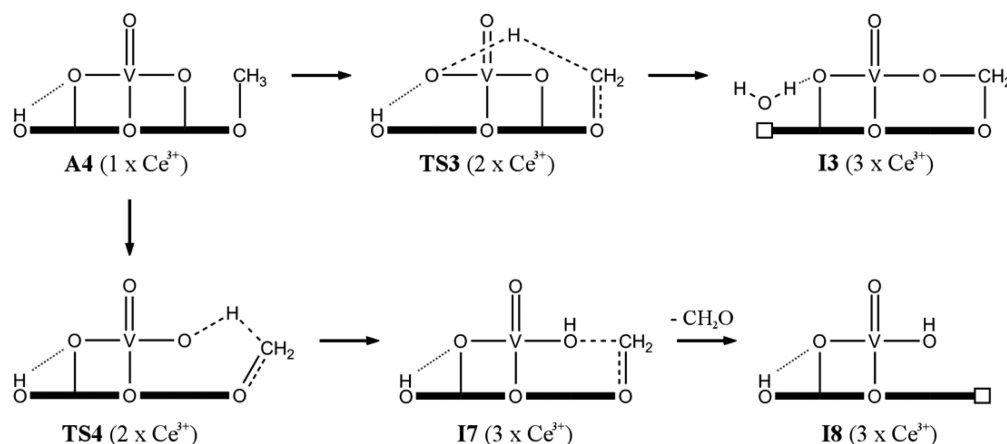
Figure 9. Reaction mechanisms for the hydrogen transfer step starting with **A4**. Top row: transfer to the more distant interphase oxygen atom; bottom row: transfer to the closer one. Dotted lines represent hydrogen bonds, whereas dashed lines represent delocalized electrons.

Table 3. Selected Bond Distances (pm) for the Structures Shown in Figure 9 Obtained with PBE+U+D

bond	A4	TS3	I3	TS4	I7
OH···O	171	185	146	178	186
V−O	176	181	177	173	169
V=O	163	163	162	163	162
V−OC	175	172	186	181	195
O−C	143	139	141	137	127
C−H	110	139	−	137	−
O−H	−	126	97	119	98

Figure 10. PBE+U+D reaction energy profile (ZPVE-corrected) for methanol oxidation from adsorption structure **A4** (methoxide in pseudovacancy). Gibbs free energies (green) have been calculated for 300 K and 0.1 MPa. For some structures, the plus sign indicates that the reported energies include gas phase molecules, e.g. CH_3OH for VO_2+.

Figure 11. Reaction pathways for the ODH of methanol at $VO_2 \cdot CeO_2(111)$.
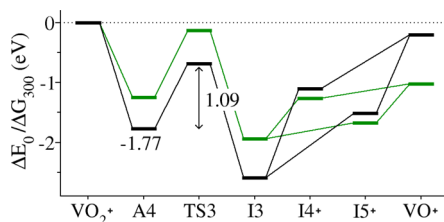

Figure 12. PBE+U+D reaction energy profile (ZPVE-corrected) for methanol oxidation from adsorption structure **A4** (methoxide in pseudovacancy). Gibbs free energies (green) have been calculated for 300 K and 0.1 MPa. For some structures, the plus sign indicates that the reported energies include gas phase molecules, e.g. CH_3OH for VO_2+.

minimum structure was found for the corresponding dihydroxide, where the interphase oxygen atom is protonated instead. Intermediate **I3** is also accessible from **A3** via **TS2**.

Figure 11 provides an overview of the different intermediates that can be reached from **A3** or **A4** on different routes. For the routes passing through **A4** and **TS3**, the desorbing formaldehyde (**I3** → **I4**, **I3** → **I5** → **VO**) contains the methanol oxygen atom and not a surface oxygen atom. Hence, no oxygen isotope exchange will be observed.

The H transfer to the closer interphase O atom via **TS4** is preferred. The transition mode (1252 cm^{-1}) also involves planarization of the CH_2O moiety. As with **TS3**, an electron is partially transferred into Ce f states. Figure 12 shows the reaction energy profile. Structures **A4**, **TS4**, and **I7** are very similar (see Table 3), and consequently, the intrinsic barrier is only 0.69 eV and the apparent barrier is particularly low (−1.08 eV).
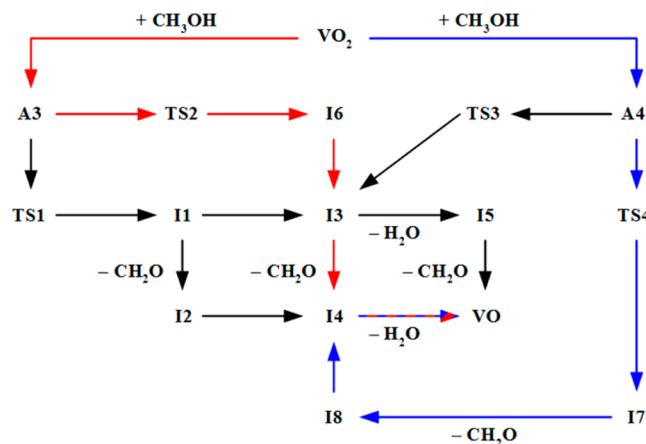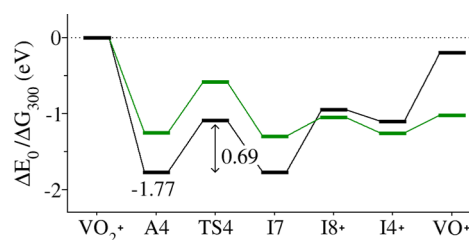
Intermediate **I7** contains a bridged V−OH···CH_2−O−Ce motif with the CH_2O fragment being structurally more similar to formaldehyde than that in **I3**. Therefore, the desorption energy amounts to 0.85 eV only. From **I7** the dihydroxyl species **I8** is reached (see Figure 9), which subsequently converts into the slightly more stable intermediate **I4** (Figure 7) via another proton transfer. The water desorption is strongly endothermic, but only mildly endergonic based on ΔG_{300}.

3.3. Hybrid Functionals. For two adsorption structures, the vanadium methoxide structure **A3** and the pseudovacancy structure **A4**, we have performed calculations using hybrid

functionals and the results are included in Table 4. The total adsorption energies show only minor systematic deviations.

Table 4. Comparison of Different Functionals for Adsorption Energies (ΔE_{ads}) for A3 and A4 as well as Intrinsic Barriers ($\Delta E^{\ddagger}$), Apparent Barriers ($\Delta E^{\ddagger}_{app}$), and Reaction Energies (ΔE_{ox}) for the Pathways Starting with A3 (All in eV)^a

	PBE+U+D	HSE+D	B3LYP+D
ΔE_{ads} (**A3**)	−1.71 (−0.29)	−1.82 (−0.14)	−1.89 (−0.40)
ΔE_{ads} (**A4**)	−1.77 (−0.32)	−1.89 (−0.21)	−2.00 (−0.49)
$\Delta E^{\ddagger}$ (**TS1**)	1.77 (+0.02)	1.82 (−0.02)	2.05 (0.00)
$\Delta E^{\ddagger}$ (**TS2**)	1.20 (−0.04)	1.53 (−0.03)	1.49 (−0.05)
$\Delta E^{\ddagger}_{app}$ (**TS1**)	0.06 (−0.27)	0.00 (−0.12)	0.16 (−0.40)
$\Delta E^{\ddagger}_{app}$ (**TS2**)	−0.51 (−0.33)	−0.29 (−0.11)	−0.40 (−0.35)
ΔE_{ox} (**I1**)	−1.04 (+0.01)	−0.63 (−0.03)	−0.65 (−0.02)
ΔE_{ox} (**I6**)	0.45 (+0.04)	0.86 (0.00)	0.83 (0.01)

^{a}Dispersion contribution in parentheses.

HSE+D and B3LYP+D predictions are about 0.1 and 0.2 eV, respectively, more exothermic than the PBE+U+D values.

The varying amounts of dispersion (about 0.2 eV for HSE, 0.3 eV for PBE+U, and 0.5 eV for B3LYP) reflect the different global scaling parameters (cf. Section 2). The dispersion correction stabilizes **A4** more strongly than **A3**, independent of the functional used. This is reasonable, as **A4** consists of methanol in a binding pocket (pseudovacancy).

For structures starting from **A3**, Table 4 also compares PBE+U+D results for intrinsic barriers, apparent barriers, and reaction energies. As expected, PBE+U+D yields lower intrinsic barriers than the hybrid functionals. The difference is about 0.3 eV for B3LYP+D (both transition structures). For HSE+D the difference is smaller for **TS1** (0.05 eV) than for **TS2** (0.33 eV). PBE+U+D reaction energies for both oxidation steps are 0.4 eV more exothermic than hybrid functional results. Dispersion has only a small effect on calculated intrinsic barriers and reaction energies (less than 0.05 eV). Due to partial compensation with differences for the adsorption energies, the PBE+U+D apparent barriers are only 0.1 eV lower than the B3LYP+D barriers, and 0.06 or 0.22 eV lower than the HSE+D barriers for **TS1** and **TS2**, respectively.

Both hybrid functionals yield the same barriers for **TS2**, but the barrier toward **TS1** is 0.2 eV higher with B3LYP. We assign this to the failure of the LYP correlation functional to describe delocalized electronic states properly.[58,59] Sauer and co-workers[21] reported that B3LYP overestimates the intrinsic barrier for an equivalent transition state on a silica support by 0.17 eV compared to CCSD(T). Adding this CCSD(T) decrement to the B3LYP result for **TS1** yields a barrier very close to the HSE result. Therefore, we believe that HSE can be considered as accurate.

4. DISCUSSION

4.1. Methanol Adsorption. With −1.7 to −1.9 eV, adsorption of methanol on $VO_2 \cdot CeO_2(111)$ is highly exothermic. This is easily understood when methanol adsorbs into the pseudovacancy (**A4**), but it is also the case when methanol binds to vanadium and replaces an anchoring surface oxygen atom, which in turn relaxes into the pseudovacancy

(**A1**, **A2**, and **A3**). Our methanol chemisorption energies for vanadia/ceria are almost 1.1 eV higher than the values reported for vanadia/silica (based on B3LYP results, cf. Table 4).[21] They are also substantially higher than the −0.51 and −0.91 eV reported for vanadia/anatase[28] and pristine ceria,[57] respectively.

To the best of our knowledge, experimental adsorption energies are not available for the low vanadia loading studied here. For vanadia loadings of 6 wt % $V_2O_5 \cdot CeO_2$, which is equivalent to 11.3 V/nm^2 and substantially exceeds the loading corresponding to a monolayer,[60] Feng and Vohs determined a methanol desorption energy of 0.83 eV.[61] This value matches the DFT (PW91) adsorption energy of −0.64 eV for methanol on $V_2O_5(001)$[62] when adding the expected dispersion contribution of −0.2 eV (see Table 1).

The V=O stretching mode is one of the characteristic vibrations of vanadia surface species.[63] For **A2**, **A3**, and **A4**, a constant V=O bond distance of 163 pm was found. In contrast to the molecular adsorption structures **A5** and **A6**, in **A2**–**A4** the V=O bond is tilted toward the surface. In addition, the dipoles of the V=O and the O−H bonds are oppositely aligned and couple, which results in a substantial loss of intensity for the V=O stretching mode. This has been demonstrated by calculating IR intensities of a hydrogenated $VO_2 \cdot CeO_2(111)$ surface model. We conclude that the extinction of the V=O stretching band upon methanol adsorption observed by Abbott et al.[12] is due to three effects: interaction with the OCH$_3$ dipole, tilting of V=O toward the surface (selection rule), and screening of the V=O dipole by the OH dipoles.

4.2. Simulation of TPD Experiments. Figure 11 shows four different pathways for the formation of formaldehyde. The calculated energy barriers in Table 5 indicate that only two may

Table 5. ZPVE- and Dispersion Corrected Intrinsic Barriers ($\Delta E^{\ddagger}$) in eV, Theoretical Desorption Temperatures T_{des} in K, Pre-exponential Factors A at T_{des}, and Kinetic Isotope Effects for the ODH of Methanol at $VO_2 \cdot CeO_2(111)$

	$\Delta E^{\ddagger}_{PBE+U+D}$	$\Delta E^{\ddagger}_{HSE+D}$	A	T_{des}	KIE
TS1	1.65	1.70	2.8×10^{12}	640	2.2
TS2	1.03	1.36	3.0×10^{12}	495	3.2
TS3	1.09	1.4^a (1.57)^b	8.3×10^{12}	510	2.3
TS4	0.69	1.0^a (1.15)^b	2.2×10^{13}	370	6.1
CeO$_2$^{c}	1.33	1.44	7.8×10^{11}	590	2.6

^{a}Estimated by adding the HSE correction from **TS2** to the PBE+U value. ^{b}In parentheses: result of single-point HSE+D calculation. ^{c}Reference 57.

be relevant: From the vanadium methoxide chemisorption structure (**A3**) via **TS2** (H transfer to oxygen of the ceria surface) and from the chemisorption structure in the pseudovacancy of CeO$_2$ (**A4**) via **TS4** (H transfer to oxygen in the V−O−Ce interphase bond).

For a more detailed comparison with the experiments by the Freund group,[12,13] temperature-programmed desorption spectra have been simulated. Note that the experiments start from dissociatively adsorbed CH$_3$OH at presaturated surfaces, i.e. in the high-coverage regime.[12,13] According to the reaction mechanisms discussed in the previous sections, the intrinsic barrier for the oxidation step $\Delta E^{\ddagger}_0$ is also the barrier for formaldehyde desorption. Assuming first-order kinetics, the desorption rate dx/dt is given by

$$-\frac{dx}{dt} = \frac{k_B T}{h} \cdot \frac{q^{\ddagger}}{q} \cdot \exp\left(-\frac{\Delta E_0^{\ddagger}}{k_B T}\right) \cdot x$$

with coverage x and temperature T as time-dependent quantities. This differential equation was solved numerically with a (constant) heating rate of 3 K/s, which was also used in the experiment. The initial coverage for each pathway was set to $x_0 = 1$. Calculated (PBE+U+D) partition functions for transition state ($q^{\ddagger}$) and adsorption complex (q) are compiled in Table 5 for the reaction pathways studied. For the barriers we use ZPVE-corrected HSE+D values, estimated by adding the HSE corrections for **TS2** to the PBE+U+D results for **TS3** and **TS4**. This seems justified because the three transition states have similar electronic structures. We have also calculated the reaction rates for fully deuterated CD_3OD in order to quantify the kinetic isotope effect KIE = k_H/k_D for each oxidation pathway.

The predicted desorption temperatures in Table 5 confirm that from **A3** only the desorption pathway via **TS2** and from **A4** only the pathway via **TS4** are relevant. The resulting desorption rates are plotted in Figure 13 along with the TPD spectrum
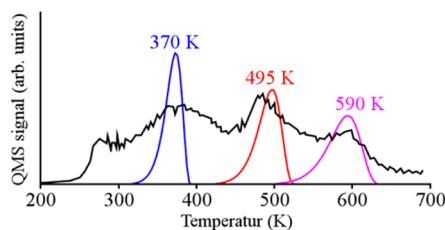

Figure 13. Experimental TPD spectrum[13] (black) along with the simulated CH_2O desorption peaks via **TS4** (blue) and **TS2** (red). The third peak (purple) originates from the defective (= oxygen vacancy) $CeO_2(111)$ surface as shown in ref 57.

recorded for monomeric vanadia clusters as published in ref 13. At vanadia loadings of around 2.7 V/nm^2, the pristine $CeO_2(111)$ surface is exposed and may contribute to the formaldehyde formation as well. Therefore, we include the desorption peak resulting from the vanadia-free surface that is discussed in ref 57. These results suggest the following peak assignments: α peak—formaldehyde formation upon chemisorption into the pseudovacancy (**TS4**), β peak—formaldehyde formation from methoxide at the vanadia surface species (**TS2**), and γ peak—formaldehyde formation on the ceria support without vanadia participation.[57] The pathway via **TS4** has the highest KIE, which is plausible, as this pathway occurs at the lowest temperature. With fully deuterated CD_3OD, the α peak occurs at 390 K.

HSE barriers are in excellent agreement with experimental barriers, which were derived by assuming a constant pre-exponential factor of 10^{13} s^{-1}. DFT frequency calculations render a calculation of pre-exponentials possible. The pre-exponential factors compiled in Table 5 show that the conventional assumption of 10^{13} s^{-1} is reasonable. In fact, we advise against blind fitting to experimental values, as it might introduce significant errors due to the simplicity of the Redhead model. For a $V_2O_5 \cdot CeO_2$ catalyst, Vohs et al.[64] fitted the formaldehyde desorption peak at 540 K with a pre-exponential factor of 2×10^7 s^{-1} and a barrier of 84 kJ/mol, which is significantly lower than values reported in the present work. However, "static" transition state theory for simulating TPD

spectra is, for example, not able to describe equilibria between different adsorption structures. This is expected to significantly broaden the peaks.

A mechanistic study of vanadia polymers and monolayer films on ceria is underway. TPD studies demonstrate that higher loadings behave differently from monomers. The missing low temperature peak[13,64] fits to the prediction of a lower activity of polymers based on oxygen defect formation energies.[20]
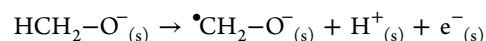
4.3. Cooperativity between Vanadia and the Support.
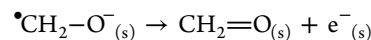The partial oxidation of methanol on supported vanadia proceeds in three steps:

(1) heterolytic splitting of CH_3OH and chemisorption of the methoxide anion,

$$HCH_2-OH \rightarrow HCH_2-O^-_{(s)} + H^+_{(s)}$$

(2) hydrogen abstraction from the methyl group,

$$HCH_2-O^-_{(s)} \rightarrow {}^\bullet CH_2-O^-_{(s)} + H^+_{(s)} + e^-_{(s)}$$

(3) formaldehyde release.

$${}^\bullet CH_2-O^-_{(s)} \rightarrow CH_2{=}O_{(s)} + e^-_{(s)}$$

Of the two hydrogen atoms that are removed from CH_3OH, one is decoupled into initial deprotonation (step 1) and final electron transfer on formation of molecular formaldehyde (step 3), whereas one is removed in a proton-coupled electron transfer step (PCET, step 2).

Different sites of the vanadia surface species are involved in the different steps. For monomeric vanadia species on silica, methanol chemisorbs at the V−O−Si interphase bond and forms a V−OCH_3 species, whereas the H atom is transferred to the V=O bond. In the transition structure, the proton is attached to the O atom, and the electron is accommodated in vanadium d states, reducing vanadium from +5 to +4 (PCET). When $CH_2{=}O$ is released, another electron is transferred to vanadium d states, creating a V^{+3} species.

For monomeric vanadia species on titania, both rutile[30,31] and anatase,[28] CH_3OH also chemisorbs at the V−O−Ti interphase bond yielding a methoxide group attached to V and an OH group attached to the support. Hydrogen transfer is most favorable to the vanadyl O atom on the rutile support,[30,31] whereas a surface O atom is the best H acceptor for vanadia/anatase.[28] In the latter case, both electrons are transferred into subsurface Ti d states.

For our vanadia/ceria system, the most favored pathway starts from methoxide adsorbed at the ceria surface in a pseudovacancy (**A4**) that is formed upon deposition of the monomeric vanadia species. When the H atom is transferred to the V−O−Ce interphase bond (**TS4**, −0.69 eV), the V−O bond gets protonated, whereas the electron is accommodated in Ce f states, creating a Ce^{3+} ion. An example with even more distant proton and electron accepting sites is selective oxidation of butane at vanadium phosphate oxide.[65,66] It has been found that the proton is transferred to P=O bonds, whereas the electron occupies vanadium d states.

Methanol may also chemisorb at the V−O−Ce interphase bond and form a V−OCH_3 species (**A3**). For the hydrogen transfer there are two options. Similarly to vanadia/silica, the H atom can be transferred to the oxygen atom of the vanadyl bond (**TS1**), but H transfer to the ceria surface yields a lower

barrier (1.03 eV). In the transition structure (**TS2**) the proton binds to an oxygen ion of the ceria surface, and the electron is accommodated in a cerium f state, reducing cerium from +4 to +3. On rearrangement of the bridging $V\cdots O(CH_2)\cdots HO$ surface structure (**I6**) into molecularly adsorbed CH_2O (**I3**), another electron is transferred into Ce f states.

In both cases, ceria is directly involved in the redox process, as two electrons are accommodated in Ce f states forming two Ce^{3+} ions whereas vanadium remains fully oxidized (V^{5+}). In previous studies[11,13] we have shown, for vanadia supported on ceria and for vanadia–ceria gas phase clusters,[67] that vanadium is always stabilized in its highest oxidation state (+5) and a Ce^{3+}/V^{5+} redox pair is always more stable than a Ce^{4+}/V^{4+} redox pair. This is a consequence of the specific coordination of the ions at this interphase and the specific relaxation possibilities and is by no means trivial. In aqueous solution there is a preference for the Ce^{3+}/V^{5+} redox pair, as the reduction potentials of 1.3–1.7 eV for Ce^{4+} and 1.0 eV for V^{5+} (in VO_2^+) indicate.[67] This is also the case for the bulk oxides as the reaction

$$CeO_2 + VO_2 \rightarrow \frac{1}{2}Ce_2O_3 + \frac{1}{2}V_2O_5 \qquad (4)$$
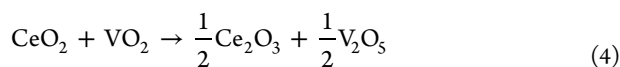
is endothermic ($\Delta H° = 1.1–1.3$ eV), whereas the formation of $CeVO_4$ is exothermic ($\Delta H° = −1.5$ eV).[68,69] As a result, transition states with (partially) populated V d states such as **TS1** are disfavored over transition states with populated Ce f states (**TS2**–**TS4**).

On the vanadia-free ceria surface, the hydrogen atom is transferred to an oxygen of the ceria surface (as in **TS2**), but from a methoxy species that is also bound to the ceria surface which results in a higher intrinsic barrier (1.44 eV, Table 5) and a higher formaldehyde desorption temperature (590 K). Note that an oxygen vacancy is needed to bind methanol strong enough that it will not desorb before hydrogen transfer occurs.[57]

On the pure V_2O_5 surface, methanol adsorption also occurs on oxygen defects only,[62] and the barriers are expected to be similar to **TS1** and to the transition structure for the vanadia/silica system, which explains the higher temperatures at which formaldehyde formation is observed (400–550 K).[62]

5. CONCLUSIONS

Compared to the vanadia/silica system, the vanadia/ceria system is a more active catalyst both because methanol binds more strongly on the surface and the intrinsic barriers for the hydrogen transfer step are lower. The reason is the direct participation of ceria in the redox process. On nonreducible supports such as silica, vanadia is reduced, whereas ceria as a support stabilizes vanadium in its highest oxidation state. Our successful simulation of two peaks observed in temperature-programmed desorption experiments confirms the prediction of two low energy pathways that involve different surface sites in the adsorption and hydrogen transfer steps.

Vanadia/ceria is also a more active catalyst than ceria alone or vanadia alone where methanol adsorption occurs at oxygen vacancies and hydrogen is transferred to a neighbored site on the oxide surface.

We conclude that support effects are complex phenomena and the role of the support goes far beyond a mere electronic polarization, as captured by electronegativity scales. Different active sites may be involved for different supports. The support

may also provide sites for binding the substrate molecules, and reducible supports may be involved in the redox process.

■ ASSOCIATED CONTENT

Ⓢ Supporting Information

Simulated vibrational spectra for **A1**–**A4**, structures of intermediates, and a table with total energies. This material is available free of charge via the Internet at http://pubs.acs.org.

■ AUTHOR INFORMATION

Corresponding Author
js@chemie.hu-berlin.de

Notes
The authors declare no competing financial interest.

■ ACKNOWLEDGMENTS

■ REFERENCES

(1) Somorjai, G. A.; Li, Y. *Introduction to Surface Chemistry and Catalysis*; John Wiley & Sons: Hoboken, NJ, 2010.
(2) Thomas, J. M.; Thomas, W. J. *Principles and Practice of Heterogeneous Catalysis*; Wiley: Weinheim, 1997.
(3) An, K.; Alayoglu, S.; Musselwhite, N.; Plamthottam, S.; Melaet, G.; Lindeman, A. E.; Somorjai, G. A. *J. Am. Chem. Soc.* **2013**, *135*, 16689.
(4) Deo, G.; Wachs, I. E. *J. Catal.* **1994**, *146*, 323.
(5) Wachs, I. E.; Deo, G.; Juskelis, M. V.; Weckhuysen, B. M. In *Dynamics of Surfaces and Reaction Kinetics in Heterogeneous Catalysis*; Froment, G. F., Waugh, K. C., Eds.; Elsevier: Amsterdam, 1997; p 305.
(6) Wachs, I. E.; Chen, Y.; Jehng, J.-M.; Briand, L. E.; Tanaka, T. *Catal. Today* **2003**, *78*, 13.
(7) Wachs, I. E. In *Catalysis*; Spivey, J. J., Ed.; The Royal Society of Chemistry: 1997; Vol. *13*, p 37.
(8) Khodakov, A.; Olthof, B.; Bell, A. T.; Iglesia, E. *J. Catal.* **1999**, *181*, 205.
(9) Beck, B.; Harth, M.; Hamilton, N. G.; Carrero, C.; Uhlrich, J. J.; Trunschke, A.; Shaikhutdinov, S.; Schubert, H.; Freund, H.-J.; Schlögl, R.; Sauer, J.; Schomäcker, R. *J. Catal.* **2012**, *296*, 120.
(10) Olthof, B.; Khodakov, A.; Bell, A. T.; Iglesia, E. *J. Phys. Chem. B* **2000**, *104*, 1516.
(11) Baron, M.; Abbott, H.; Bondarchuk, O.; Stacchiola, D.; Uhl, A.; Shaikhutdinov, S.; Freund, H.-J.; Popa, C.; Ganduglia-Pirovano, M. V.; Sauer, J. *Angew. Chem., Int. Ed.* **2009**, *48*, 8006.
(12) Abbott, H. L.; Uhl, A.; Baron, M.; Lei, Y.; Meyer, R. J.; Stacchiola, D. J.; Bondarchuk, O.; Shaikhutdinov, S.; Freund, H. J. *J. Catal.* **2010**, *272*, 82.
(13) Ganduglia-Pirovano, M. V.; Popa, C.; Sauer, J.; Abbott, H. L.; Uhl, A.; Baron, M.; Stacchiola, D.; Bondarchuk, O.; Shaikhutdinov, S.; Freund, H.-J. *J. Am. Chem. Soc.* **2010**, *132*, 2345.
(14) Paier, J.; Penschke, C.; Sauer, J. *Chem. Rev.* **2013**, *113*, 3949.
(15) McQuarters, A. B.; Wolf, M. W.; Hunt, A. P.; Lehnert, N. *Angew. Chem., Int. Ed.* **2014**, *53*, 4750.
(16) Wachs, I. E. *Catal. Today* **2005**, *100*, 79.
(17) Sauer, J.; Döbler, J. *Dalton Trans.* **2004**, *19*, 3116.
(18) Kim, H. Y.; Lee, H. M.; Pala, R. G. S.; Shapovalov, V.; Metiu, H. *J. Phys. Chem. C* **2008**, *112*, 12398.

(19) Rozanska, X.; Fortrie, R.; Sauer, J. *J. Am. Chem. Soc.* **2014**, *136*, 7751.

(20) Penschke, C.; Paier, J.; Sauer, J. *J. Phys. Chem. C* **2013**, *117*, 5274.

(21) Döbler, J.; Pritzsche, M.; Sauer, J. *J. Am. Chem. Soc.* **2005**, *127*, 10861.

(22) Bronkema, J. L.; Bell, A. T. *J. Phys. Chem. C* **2007**, *111*, 420.

(23) Burcham, L. J.; Wachs, I. E. *Catal. Today* **1999**, *49*, 467.

(24) Mars, P.; van Krevelen, D. W. *Chem. Eng. Sci.* **1954**, *3* (Supplement 1), 41.

(25) Rozanska, X.; Kondratenko, E. V.; Sauer, J. *J. Catal.* **2008**, *256*, 84.

(26) Popa, C.; Ganduglia-Pirovano, M. V.; Sauer, J. *J. Phys. Chem. C* **2011**, *115*, 7399.

(27) Paier, J.; Kropp, T.; Penschke, C.; Sauer, J. *Faraday Discuss.* **2013**, *162*, 233.

(28) Shapovalov, V.; Fievez, T.; Bell, A. T. *J. Phys. Chem. C* **2012**, *116*, 18728.

(29) Goodrow, A.; Bell, A. T. *J. Phys. Chem. C* **2008**, *112*, 13204.

(30) Kim, H. Y.; Lee, H. M.; Pala, R. G. S.; Metiu, H. *J. Phys. Chem. C* **2009**, *113*, 16083.

(31) Kim, H. Y.; Lee, H. M.; Metiu, H. *J. Phys. Chem. C* **2010**, *114*, 13736.

(32) Ernzerhof, M.; Scuseria, G. E. *J. Chem. Phys.* **1999**, *110*, 5029.

(33) Grimme, S. *J. Comput. Chem.* **2006**, *27*, 1787.

(34) Kerber, T.; Sierka, M.; Sauer, J. *J. Comput. Chem.* **2008**, *29*, 2088.

(35) Anisimov, V. I.; Zaanen, J.; Andersen, O. K. *Phys. Rev. B* **1991**, *44*, 943.

(36) Liechtenstein, A. I.; Anisimov, V. I.; Zaanen, J. *Phys. Rev. B* **1995**, *52*, R5467.

(37) Blöchl, P. E. *Phys. Rev. B* **1994**, *50*, 17953.

(38) Kresse, G.; Joubert, D. *Phys. Rev. B* **1999**, *59*, 1758.

(39) Kresse, G.; Furthmüller, J. *Phys. Rev. B* **1996**, *54*, 11169.

(40) Kresse, G.; Furthmüller, J. *Comput. Mater. Sci.* **1996**, *6*, 15.

(41) Perdew, J. P.; Ernzerhof, M.; Burke, K. *J. Chem. Phys.* **1996**, *105*, 9982.

(42) Fabris, S.; Vicario, G.; Balducci, G.; de Gironcoli, S.; Baroni, S. *J. Phys. Chem. B* **2005**, *109*, 22860.

(43) Castleton, C. W. M.; Kullgren, J.; Hermansson, K. *J. Chem. Phys.* **2007**, *127*, 244704.

(44) Dudarev, S. L.; Botton, G. A.; Savrasov, S. Y.; Humphreys, C. J.; Sutton, A. P. *Phys. Rev. B* **1998**, *57*, 1505.

(45) Bengone, O.; Alouani, M.; Blöchl, P.; Hugel, J. *Phys. Rev. B* **2000**, *62*, 16392.

(46) Heyd, J.; Scuseria, G. E.; Ernzerhof, M. *J. Chem. Phys.* **2003**, *118*, 8207.

(47) Becke, A. D. *J. Chem. Phys.* **1993**, *98*, 5648.

(48) Lee, C.; Yang, W.; Parr, R. G. *Phys. Rev. B* **1988**, *37*, 785.

(49) Mills, G.; Jonsson, H.; Schenter, G. K. *Surf. Sci.* **1995**, *324*, 305.

(50) Jonsson, H.; Mills, G.; Jacobsen, K. W. In *Classical and Quantum Dynamics in Condensed Phase Simulations*; Berne, J., Ciccotti, G., Coker, D. F., Eds.; World Scientific: Singapore, 1998; p 385.

(51) Henkelman, G.; Uberuaga, B. P.; Jonsson, H. *J. Chem. Phys.* **2000**, *113*, 9901.

(52) Henkelman, G.; Jonsson, H. *J. Chem. Phys.* **1999**, *111*, 7010.

(53) Heyden, A.; Bell, A. T.; Keil, F. J. *J. Chem. Phys.* **2005**, *123*, 224101.

(54) Momma, K.; Izumi, F. *J. Appl. Crystallogr.* **2011**, *44*, 1272.

(55) Watkins, M. B.; Foster, A. S.; Shluger, A. L. *J. Phys. Chem. C* **2007**, *111*, 15337.

(56) Romanyshyn, Y.; Guimond, S.; Kuhlenbeck, H.; Kaya, S.; Blum, R. P.; Niehus, H.; Shaikhutdinov, S.; Simic-Milosevic, V.; Nilius, N.; Freund, H. J.; Ganduglia-Pirovano, M. V.; Fortrie, R.; Döbler, J.; Sauer, J. *Top. Catal.* **2008**, *50*, 106.

(57) Kropp, T.; Paier, J. *J. Phys. Chem. C* **2014**, DOI: 10.1021/jp505088b.

(58) Kurth, S.; Perdew, J. P.; Blaha, P. *Int. J. Quantum Chem.* **1999**, *75*, 889.

(59) Paier, J.; Marsman, M.; Kresse, G. *J. Chem. Phys.* **2007**, *127*, 024103.

(60) Wachs, I. E. *Dalton Trans.* **2013**, *42*, 11762.

(61) Feng, T.; Vohs, J. M. *J. Catal.* **2004**, *221*, 619.

(62) Sturm, J. M.; Göbke, D.; Kuhlenbeck, H.; Döbler, J.; Reinhardt, U.; Ganduglia-Pirovano, M. V.; Sauer, J.; Freund, H. *J. Phys. Chem. Chem. Phys.* **2009**, *11*, 3290.

(63) Magg, N.; Immaraporn, B.; Giorgi, J. B.; Schroeder, T.; Bäumer, M.; Döbler, J.; Wu, Z. L.; Kondratenko, E.; Cherian, M.; Baerns, M.; Stair, P. C.; Sauer, J.; Freund, H. J. *J. Catal.* **2004**, *226*, 88.

(64) Wong, G. S.; Concepcion, M. R.; Vohs, J. M. *J. Phys. Chem. B* **2002**, *106*, 6451.

(65) Cheng, M.-J.; Nielsen, R. J.; Tahir-Kheli, J.; Goddard, W. A., III. *Phys. Chem. Chem. Phys.* **2011**, *13*, 9831.

(66) Cheng, M.-J.; Goddard, W. A., III. *J. Am. Chem. Soc.* **2013**, *135*, 4600.

(67) Jiang, L.; Wende, T.; Claes, P.; Bhattacharyya, S.; Sierka, M.; Meijer, G.; Lievens, P.; Sauer, J.; Asmis, K. R. *J. Phys. Chem. A* **2011**, *115*, 11187.

(68) Da Silva, J. L. F.; Ganduglia-Pirovano, M. V.; Sauer, J. *Phys. Rev. B* **2007**, *76*, 125117.

(69) Da Silva, J. L. F.; Ganduglia-Pirovano, M. V.; Sauer, J.; Bayer, V.; Kresse, G. *Phys. Rev. B* **2007**, *75*, 045121.